Electrodes Optimization of an Annular Flow Electromagnetic Measurement System for Drilling Engineering

LIANG GE[1,3]**, DAN LI**[1]**, QI HUANG**[1]**, (Student Member, IEEE), GUIYUN TIAN**[2]**, (Senior Member, IEEE), GUOHUI WEI**[1]**, AND JUNAID AHMED**[4]

[1]College of Mechanical and Electronic Engineering, Southwest Petroleum University, Chengdu 610500, China
[2]School of Engineering, Newcastle University, Newcastle NE1 7RU, U.K.
[3]Research Institute of Artificial Intelligence, Southwest Petroleum University, Chengdu 610500, China
[4]Electrical Department, Sukkur IBA University, Sukkur 65200, Pakistan

Corresponding author: Guiyun Tian (g.y.tian@ncl.ac.uk)

ABSTRACT The early monitoring of downhole overflow can be effectively realized by the downhole annular electromagnetic flow detection system. In order to improve the accuracy of the electromagnetic measurement system of downhole annular flow, it is important to optimize the excitation system and electrodes of this system. This research focuses on the optimization of the electrodes for the electromagnetic measurement system of downhole annular flow, whose excitation system has been optimized. First, the basic principle of electromagnetic measurement of downhole annular flow is analyzed. Then, the influence of different positions of the four-point electrodes on the virtual current distributions is analyzed, and the optimum electrode positions and distributions are introduced. On this basis, the influence of shape and size of the large electrode on virtual current density distribution is analyzed. Based on the theoretical study of the influence of electrode on virtual current density distribution, taking hemispherical electrodes and arc electrodes as examples, this paper optimizes hemispherical electrodes and arc electrodes with different shapes and sizes by using finite element simulation method, and proposes three indexes to evaluate the annular virtual current density distributions when the electrodes of different shapes are used. The optimum parameters of shapes and sizes of the hemisphere electrodes and arc electrodes under specific structures of the downhole annular electromagnetic flow measurement system are obtained. This research has great significance for the optimization of electrodes in the downhole annular electromagnetic flow measurement system, and can also be used as reference for the electrode optimization of the traditional electromagnetic flowmeter.

INDEX TERMS Electrode design, optimization simulation, finite element simulation, annular flow, electromagnetic measurement.

I. INTRODUCTION

With the development of the world economy, the demand of countries around the world for energy is increasing, and the oil exploration and development has been expanding continuously. The difficulties of drilling wells are ascending [1]. The development of complex areas easily causes the

The associate editor coordinating the review of this manuscript and approving it for publication was Chaitanya U. Kshirsagar.

high-pressure problems. Blowout is a phenomenon where the pressure of the underground fluids is larger than that of the wellbore pressure so that the underground fluids influx into the well and spurt out of the ground. Blowout is very harmful, which not only contaminates the environment, but also causes huge economic losses, tragic accidents and heavy casualties. As the precursor of blowout, overflow causes rapid variations of the downhole annular flow. Therefore, the annular flow monitoring is very important [2]

Due to the reliable and simple structure, immovable parts, strong anti-corrosion ability, no congestions and no pressure loss, the electromagnetic measurement can be used for downhole annular flow measurement [3]. The main components of the electromagnetic flow measurement system are the excitation system and the electrodes. The excitation system generates a magnetic field, and the electrodes acquire electromagnetic induction signals of the flow. By optimizing the excitation system, a relatively uniform magnetic field can be obtained, and the optimized electrode can make the measurement signal more accurate. Therefore, the optimization of the excitation system and the electrode have been hotly researched by scholars [4]–[7]. The shape and size of the excitation coil are mainly researched in the area of excitation optimization and design. However, the design of excitation system is limited in space under special annular environment [8]. Therefore, this study is aimed at the optimization of the electrode of the downhole annular electromagnetic measurement equipment through theoretical research, finite element simulation and data evaluation.

The electrode directly determines the distribution of the virtual current density of the annular flow electromagnetic measurement system, thus affecting the output signal measurement. Traditional electrodes are point electrodes and large electrodes. Point electrodes are widely used for axis-symmetric single-phase flow parameter measurement of pipeline fluids, while large electrodes can measure non-axisymmetric flow, multi-phase flow, and non-full flow. At present, there are many researches on electrode optimization and design, including the number, position and structure size of the electrodes. In 1998, Horner B began to study the industrial multi-electrode electromagnetic flowmeter [8], which played a key role in improving the accuracy of electromagnetic flow measurement. In 2000, Lucas G P proposed a six-electrode electromagnetic flow measurement system [9]. The system achieved good measurement results in the measurement of solid-liquid two-phase flow. In 2002, X.Z.Zhang used the alternating iterative method to analyze the three-dimensional characteristics of the virtual current of a cylindrical electromagnetic flowmeter when a bubble is contained, but only in the case of two point electrodes [10]. In 2004, H.J.Zhang of Zhejiang University proposed a cylindrical electromagnetic flowmeter with 8 electrodes, and concluded that multi-electrode electromagnetic flowmeter can almost eliminate the influence of flow rate non-symmetry of the measurement results [11]. G.Y.Zhang proposed a new four electrode outflow electromagnetic flowmeter, and verified the consistency between the result and experiment of finite element simulation, which further illustrated that the error of simulation and experiment results is relatively small when the flow rate is large. However, he did not conduct any theoretical studies [12]. Y.Y.Zhao proposed the concept of area weight function based on Shercliff weight function, and used 16 electrodes to measure the double-phased non-symmetric flow [13], [14].

When the flow rate is asymmetrically distributed, extremely large measurement error can be easily caused. In order to satisfy the measurement requirement of double-phased and asymmetric flow and improve the electrode sensitivity to the flow rate distributions, many scholars proposed multi-electrode and arc electrode to measure double-phase fluid, asymmetric flow, or non-full pipe flow. In theory, the more electrodes are used in sensors, the better the measurement accuracy and stability of the electromagnetic flowmeter will be. However, increasing the number of electrodes means increasing amplification circuit, the expense and the difficulty to make sensors. In practical applications, the majority of target electrodes can be replaced by a smaller number of large electrodes. In 2014, Leeungculsatier and Kollr proposed the method of reconstructing velocity distribution by using multi-electrode electromagnetic flowmeter [15], [16]. In 2014, Y.Y.Shi designed an electromagnetic flowmeter measurement system with arc electrodes, explained the excellent linear relationship between the induced voltage of arc electrodes and the fluid parameters, and optimized the tension angles of two arc electrodes [17]. In 2015, L.F.Kong used finite element method to optimize the number and position of electrodes. He proposed that the 6-electrode electromagnetic flowmeter was superior to the 2-electrode electromagnetic flowmeter in terms of uniformity of weight function distribution and average strength, but did not optimize its size and shape [18].

At present, electrode optimization is hotly researched by many scholars. However, under the special measurement environment (high temperature, high pressure and strong vibration environment) of underground annulus flow [19], if too many electrodes are used, it is not conducive to the tightness and reliability of the downhole measurement system. The electrode optimization can be realized by improving the electrode shape and excitation method [20]. In addition, many researches have been implemented based on virtual current density, but they all aimed at circular pipelines. No research has been done on electrode optimization for the virtual current density of the annular flow channel under the action of electrodes.

Therefore, this study is mainly aimed at optimizing the measuring electrode in the 4-electrode structure of the underground annular flow electromagnetic measurement process and obtaining the optimal electrode structure parameters. The following structure is organized as follows: the second part introduces the analysis of the basic theory of downhole annular flow electromagnetic measurement, and studies the influence of the positions of four-point electrodes on virtual current distributions. Based on this study, the influence of large electrode size on current density is analyzed; in the third part hemisphere electrodes and arc electrodes of different shapes and sizes are optimized by using finite element simulation; the fourth part proposes three evaluation standards of optimization to review the annular virtual current density distributions of electrodes of different shapes and sizes. The fifth part contains the conclusion.

II. THEORETICAL RESEARCH ON ELECTRODE OPTIMIZATION

A. BASIC THEORY OF DOWNHOLE ANNULAR FLOW ELECTROMAGNETIC MEASUREMENT SYSTEM

Based on Faraday's law of electromagnetic induction, the ideal output induction electromotive force for an ideal laminar flow circle channel is expressed as [21]:

$$E = BD\overline{v} \qquad (1)$$

where E is the electromotive force, B is the magnetic induction intensity, D is the conductor length, v is the average velocity of conductor movement.

Equation (1) illustrates that the amplitude of the induction electromotive force is proportional to the magnetic induction B, the length D of the conductor, and the average velocity of the conductor motion.

When the magnetic induction intensity in the flow channel is constant, the induction electromotive force generated on the electrode is only related to the average flow rate and has a linear relationship with the flow rate, which can be expressed by equation (2):

$$E_i = C\overline{v} \qquad (2)$$

where C is a constant.

However, for the underground annular flow electromagnetic measurement system, it is difficult to form a uniform magnetic induction intensity in the annular flow channel, and during the drilling process, the underground environment conditions are complicated. The flow velocity of the annular flow channel may not be symmetrically distributed. These influences the accuracy of downhole flow electromagnetic measurement system.

For the underground annular flow electromagnetic measurement system, the optimization of the underground annular flow electromagnetic measurement system cannot be realized based on the traditional theory. In 1970, Bevir proposed the concept of three-dimensional weight vector [22]. The output induction electromotive force of the annular flow electromagnetic measurement system satisfies the basic equation of equation (3):

$$\varphi_{AB} = \int_{\tau} W \cdot \overline{v}d\tau \qquad (3)$$

where, $W = B \times j$.

φ_{AB} is the potential difference of 2 signal electrodes, W is the weight function, $\overline{v}$ is the flow rate of the drilling fluids, τ is the annular space of conductive solution, B is the magnetic intensity, and j is the virtual current density vector.

Based on this theory, if the vector weight function can be constant, the output voltage of the underground annular flow electromagnetic measurement system is only related to the integral of the flow velocity in the annular flow channel, rather than the distribution of the flow velocity. It can effectively improve the accuracy of downhole annular flow measurement. The magnetic induction intensity is determined by the physical structure size and excitation current of the
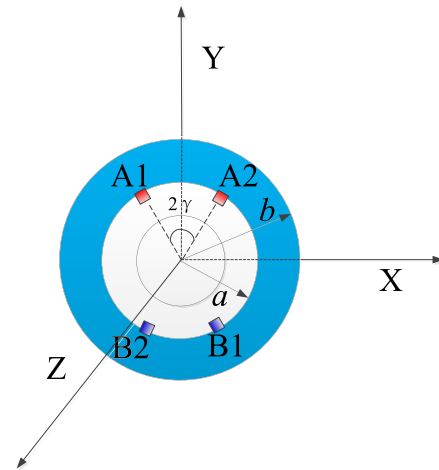

FIGURE 1. Cross-sectional diagram of annular flow measurement system with two pairs of electrodes.

excitation coil, and L.Ge has already conducted research and design [23]. So this paper only researches on the virtual current density vector of the downhole annular electromagnetic flow measurement system with nearly determined sizes and structures. The virtual current density vector is related to the geometric shape of the measurement annulus as well as positions and shape distributions of the electrode, so it's important to solve the virtual current density vector under different shapes of electrodes.

B. VECTOR DISTRIBUTION OF VIRTUAL CURRENT DENSITY AT FOUR ELECTRODES

Virtual current density is an important quantity in the theory of electromagnetic flow measurement, and it has a close relationship with the weight function. For an object whose geometric measurement annular shape and annular fluid properties are basically determined, the location distribution, shape and size of the electrodes directly determine the distribution of virtual current density. At present, there are many kinds of electrode designs, including design of single-pair electrode and multi-pair electrode, as well as point-electrode design and large-electrode design. Typical large electrodes include hemisphere electrode and arc electrode. In order to facilitate analysis and calculations [24], this section first studies the effect of electrode position distribution on virtual current density vector with four point electrodes as the research object.

The cross-sectional diagram of the annular flow measurement system with double pair electrodes (double pair coils) is shown in Figure 1. Drilling fluid flows out along the annular area between the external surface of the annular flow measurement system and the borehole wall (the Z-axis positive direction). Two pairs of electrodes (A1, A2, B1 and B2) are placed on the inner wall of the annular flow electromagnetic measurement system and directly contact with the fluid in the annular flow channel through the internal wall.

(1) Situation 1: There are two pairs of electrodes, and the half angle between two electrodes is $\gamma = 20°$, which are symmetric to the axis y. When two electrodes are placed at the positive part of the y axis and the other two negative part, the virtual current potential G satisfies the boundary condition:

$$\left.\frac{\partial G}{\partial r}\right|_{r=a} = \begin{cases} \delta\left(\phi - \frac{\pi}{2} + \gamma\right)\Big/(2a) \\ \delta\left(\phi - \frac{\pi}{2} - \gamma\right)\Big/(2a) \\ -\delta\left(\phi + \frac{\pi}{2} + \gamma\right)\Big/(2a) \\ -\delta\left(\phi + \frac{\pi}{2} - \gamma\right)\Big/(2a) \end{cases} \quad (4)$$

The general solution of virtual current potential is shown in equation (5), and the partial derivative of it is equation (6).

$$G = C_0 + \sum_{n=1}^{\infty} C_n\left(r^n + b^{2n}r^{-n}\right)(A_n \sin n\phi + B_n \cos n\phi) \quad (5)$$

$$\frac{\partial G}{\partial r} = \sum_{n=1}^{\infty} nr^{-n-1}C_n\left(r^{2n} - b^{2n}\right)(A_n \sin n\phi + B_n \cos n\phi) \quad (6)$$

Substitute the boundary condition into equation (6):

$$\begin{aligned} A_n &= \frac{a^n}{n\pi C_n\left(a^{2n} - b^{2n}\right)} \\ &\quad \times \left[\sin\left(n\left(\frac{\pi}{2} - \gamma\right)\right) + \sin\left(n\left(\frac{\pi}{2} + \gamma\right)\right)\right] \\ &= \frac{2a^n \sin(n\pi/2)\cos n\gamma}{n\pi C_n\left(a^{2n} - b^{2n}\right)} \end{aligned} \quad (7)$$

$$B_n = 0 \quad (8)$$

Substitute the coefficient expressions (7) and (8) into (6):

$$\begin{aligned} G(r,\phi) &= \frac{2}{\pi}\sum_{n=1,3,5}^{\infty} \frac{(a/b)^n (r/b)^n + (a/r)^n}{n\left[(a/b)^{2n} - 1\right]}\cos n\gamma \\ &\quad \times \cos[n(\phi - \pi/2)] \end{aligned} \quad (9)$$

The positions of electrodes are shown Figure 1. The positive electrodes A1 and A2 (angle of tension 2γ), the negative electrodes B1 and B2 (angle of tension 2γ), are symmetrical to y axis. According to equation (9), virtual current potential contours (black lines) and virtual current streamlines (red lines) in Figures 2 (a), 2 (b), 2 (c) and 2 (d) are plotted, In Figure (a) and Figure (b) $2\gamma = 30°$, while in Figure c and Figure (d)$2\gamma = 80°$. It can be seen from Fig. 2 that as the angle of the electrode increases, the uniformity of the virtual current potential increases significantly.

(2) Situation 2: If the two pairs of electrodes are arranged in the order of positive, negative, positive negative, the virtual current potential function satisfies the bound condition shown
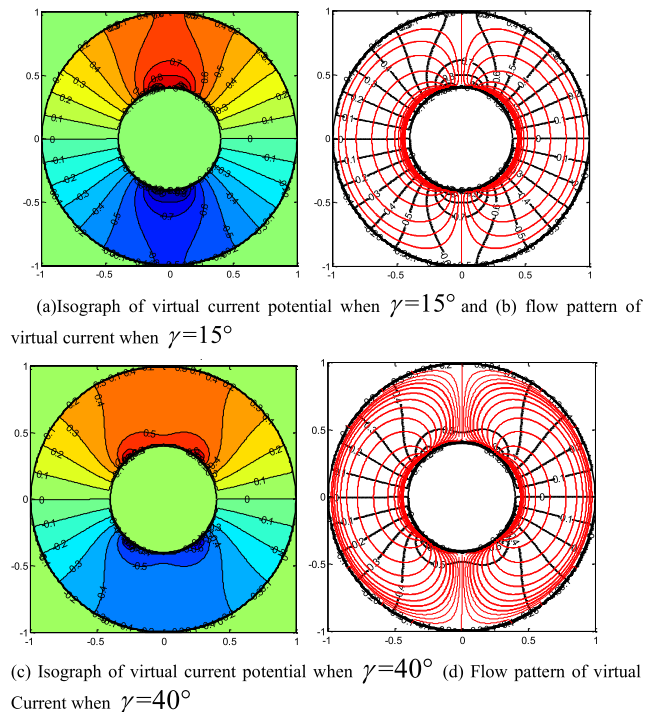

(a)Isograph of virtual current potential when $\gamma = 15°$ and (b) flow pattern of virtual current when $\gamma = 15°$

(c) Isograph of virtual current potential when $\gamma = 40°$ (d) Flow pattern of virtual Current when $\gamma = 40°$

FIGURE 2. Isograph of virtual current potential and flow pattern of virtual Current.

in equation (10):

$$\left.\frac{\partial G}{\partial r}\right|_{r=a} = \begin{cases} \delta\left(\phi - \frac{\pi}{2} + \gamma\right)\Big/(2a) \\ -\delta\left(\phi - \frac{\pi}{2} - \gamma\right)\Big/(2a) \\ \delta\left(\phi + \frac{\pi}{2} + \gamma\right)\Big/(2a) \\ -\delta\left(\phi + \frac{\pi}{2} - \gamma\right)\Big/(2a) \end{cases} \quad (10)$$

Substitute the boundary condition into virtual current general solution:

$$B_n = 0 \quad (11)$$

$$\begin{aligned} A_n &= \frac{a^n}{n\pi C_n\left(a^{2n} - b^{2n}\right)} \\ &\quad \times \left[\sin\left(n\left(\frac{\pi}{2} - \gamma\right)\right) - \sin\left(n\left(\frac{\pi}{2} + \gamma\right)\right)\right] \\ &= -\frac{2a^n \cos(n\pi/2)\sin n\gamma}{n\pi C_n\left(a^{2n} - b^{2n}\right)} \end{aligned} \quad (12)$$

The general solution can be obtained by substituting the coefficient into the virtual current potential:

$$\begin{aligned} G(r,\phi) &= -\frac{2}{\pi}\sum_{n=2,4,6}^{\infty} \frac{(a/b)^n (r/b)^n + (a/r)^n}{n\left[(a/b)^{2n} - 1\right]}\sin(n\gamma) \\ &\quad \times \sin n\left(\phi + \frac{\pi}{2}\right) \end{aligned} \quad (13)$$

$R = r/b$, and $\tau = a/b$, equation (11) can be obtained

$$G(r,\phi) = -\frac{2}{\pi}\sum_{n=2,4,6}^{\infty} \frac{R^n + R^{-n}}{n\left[\tau^n - \tau^{-n}\right]}\sin(n\gamma)\sin n\left(\phi + \frac{\pi}{2}\right) \quad (14)$$

When the electrodes are placed according to Figure 1, A1 and B1 are positive electrodes, while A2 and B2 negative electrodes. According to Formula (13), virtual current potential contours (black lines) and virtual current streamlines (red lines) are drawn, and the tension angles are ranging from 60 degree to 120 degree.

According to figure 3, it can be seen that the position of electrode has a great influence on the virtual current density distribution. When aligned in the order of positive, positive, negative, and negative, the corresponding two pairs of electrodes can also be arranged in such order, which can achieve low inhomogeneity in smaller areas. In addition, through the model analysis, when the angle between the electrodes 2γ is increased from $60°$ to $90°$, the area with uniform virtual current potential increases, and when the angle between the electrodes is increased from $90°$ to $120°$, the area with uniform virtual current potential decreases, so $90°$ is the best distribution angle.

C. VIRTUAL CURRENT DENSITY DISTRIBUTION OF HEMISPHERE AND ARC ELECTRODE

For hemispherical or arc electrodes, the line electrodes with an angle of 2γ can be composed of M point electrodes. The boundary conditions of virtual current potential are shown below:

$$\frac{\partial G}{\partial r}\bigg|_{r=a} = \begin{cases} \dfrac{1}{Ma} \displaystyle\sum_{m=0}^{M-1} \delta\left(\phi - \left[\dfrac{\pi}{2} - \gamma + \dfrac{2\gamma}{M-1}m\right]\right) \\ -\dfrac{1}{Ma} \displaystyle\sum_{m=0}^{M-1} \delta\left(\phi + \left[\dfrac{\pi}{2} + \gamma - \dfrac{2\gamma}{M-1}m\right]\right) \end{cases} \tag{15}$$

The r-direction derivative can be obtained by substituting equation (15) into into the general solution of virtual current potential:

$$\frac{\partial G}{\partial r} = \sum_{n=1}^{\infty} n r^{-n-1} C_n \left(r^{2n} - b^{2n}\right) \left(A_n \sin n\phi + B_n \cos n\phi\right) \tag{16}$$

By integrating $\sin n\phi$ or $\cos n\phi$, the following equation can be obtained:

$$A_n = \frac{a^n}{M\pi n C_n \left(a^{2n} - b^{2n}\right)}$$

$$\times \left[\sum_{m=0}^{M-1} \sin n\left(\frac{\pi}{2} - \gamma + \frac{2\gamma}{M-1}m\right)\right.$$

$$\left. + \sum_{m=0}^{M-1} \sin n\left(\frac{\pi}{2} + \gamma - \frac{2\gamma}{M-1}m\right)\right]$$

$$= \frac{2a^n \sin\frac{n\pi}{2} \displaystyle\sum_{m=0}^{M-1} \cos\left(\gamma - \frac{2\gamma}{M-1}m\right)}{M\pi n C_n \left(a^{2n} - b^{2n}\right)} \tag{17}$$

$$B_n = \frac{a^n}{M\pi n C_n \left(a^{2n} - b^{2n}\right)} \left[\sum_{m=0}^{M-1} \cos n\left(\frac{\pi}{2} - \gamma + \frac{2\gamma}{M-1}m\right)\right.$$
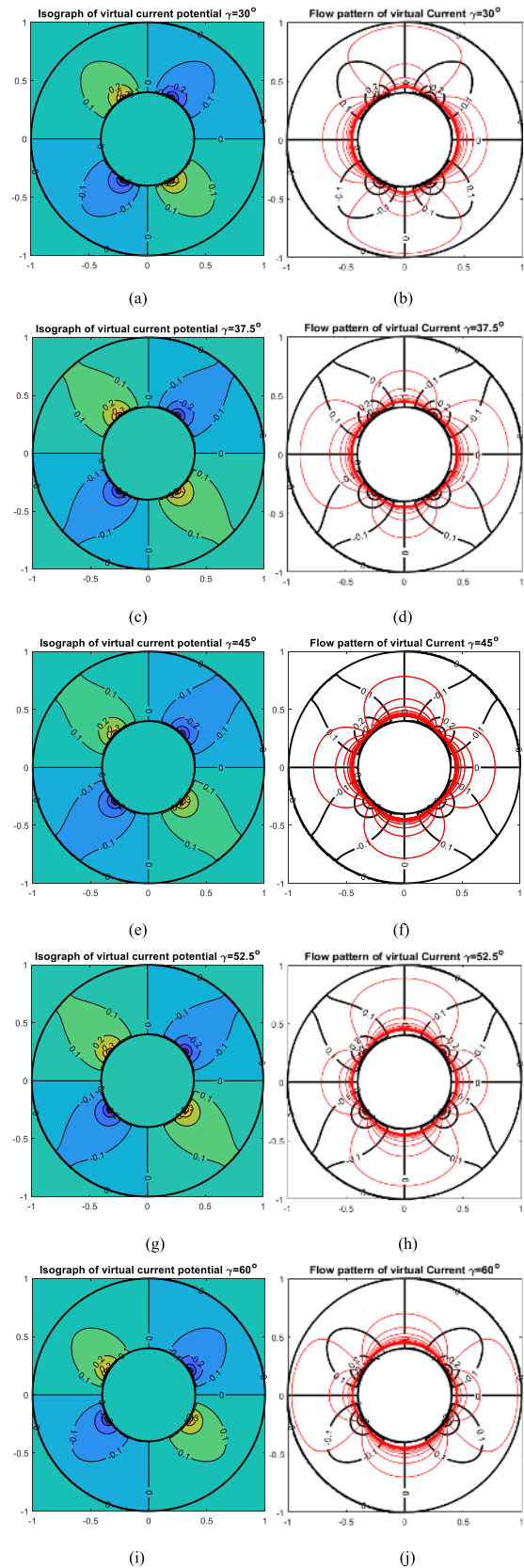

(a)   **(b)**

(c)   **(d)**

(e)   **(f)**

(g)   **(h)**

(i)   **(j)**

FIGURE 3. Virtual current potential isograph and virtual current streamline graph.

$$-\sum_{m=0}^{M-1} \cos n \left(\frac{\pi}{2} + \gamma - \frac{2\gamma}{M-1} m \right) \Bigg]$$

$$= \frac{2a^n \sin \frac{n\pi}{2} \sum_{m=0}^{M-1} \sin \left(\gamma - \frac{2\gamma}{M-1} m \right)}{M \pi n C_n \left(a^{2n} - b^{2n} \right)} \quad (18)$$

$\gamma_m = \gamma (1 - 2m/(M-1))$, and substituting it into the general solution of the virtual current potential:

$$G = \sum_{n=1}^{\infty} C_n \left(r^n + b^{2n} r^{-n} \right) (A_n \sin n\phi + B_n \cos n\phi) \quad (19)$$

$$G = \frac{2}{M\pi} \sum_{n=1,3,5}^{\infty} \frac{a^n \left(r^n + b^{2n} r^{-n} \right)}{n \left(a^{2n} - b^{2n} \right)}$$

$$\sin \frac{n\pi}{2} \sum_{m=0}^{M-1} (\cos n\gamma_m \sin n\phi + \sin n\gamma_m \cos n\phi) \quad (20)$$

$$G = \frac{2}{M\pi} \sum_{n=1,3,5}^{\infty} \frac{a^n \left(r^n + b^{2n} r^{-n} \right)}{n \left(a^{2n} - b^{2n} \right)} \sin \frac{n\pi}{2} \sum_{m=0}^{M-1} \sin n(\phi + \gamma_m) \quad (21)$$

where $R = r/b$, and $\tau = a/b$. According to equation (21), Figure 4 can be obtained, which are the virtual current potential isograph (black) and virtual current streamline diagram (red) for different number of point electrodes (M = 2, 3, 5, 10, 20).

According to the virtual current density distribution figure 4, it can be seen that the virtual current potential distribution tends to be stable when the number of point electrodes is ten. This conforms to the basic physical law, and also verifies the rationality of the virtual current potential theory of the virtual current density distribution of hemispherical or arc electrodes.

III. ELECTRODE OPTIMIZATION AND SIMULATION OF ANNULAR FLOW ELECTROMAGNETIC MEASUREMENT SYSTEM

Though the influence of the electrode position, shape and size on the virtual current density distribution has been analyzed, the optimum position of four electrodes solved and the influence of shape and size on the virtual current density obtained, it is still hard to obtain the optimum shape of the electrode. Even if the shape has been obtained, manufacturing can be really difficult and complex. However, with the development of the finite element analysis, relatively accurate optimization and design can be realized by numerical fitting. Therefore, this research aims at the two most common hemisphere and arc large electrodes. Based on the electrode distributions obtained by the previous analysis, COMSOL finite element simulations can be applied for optimizing design. Figures 5 and 6 are the three-dimensional model of the two electrodes.
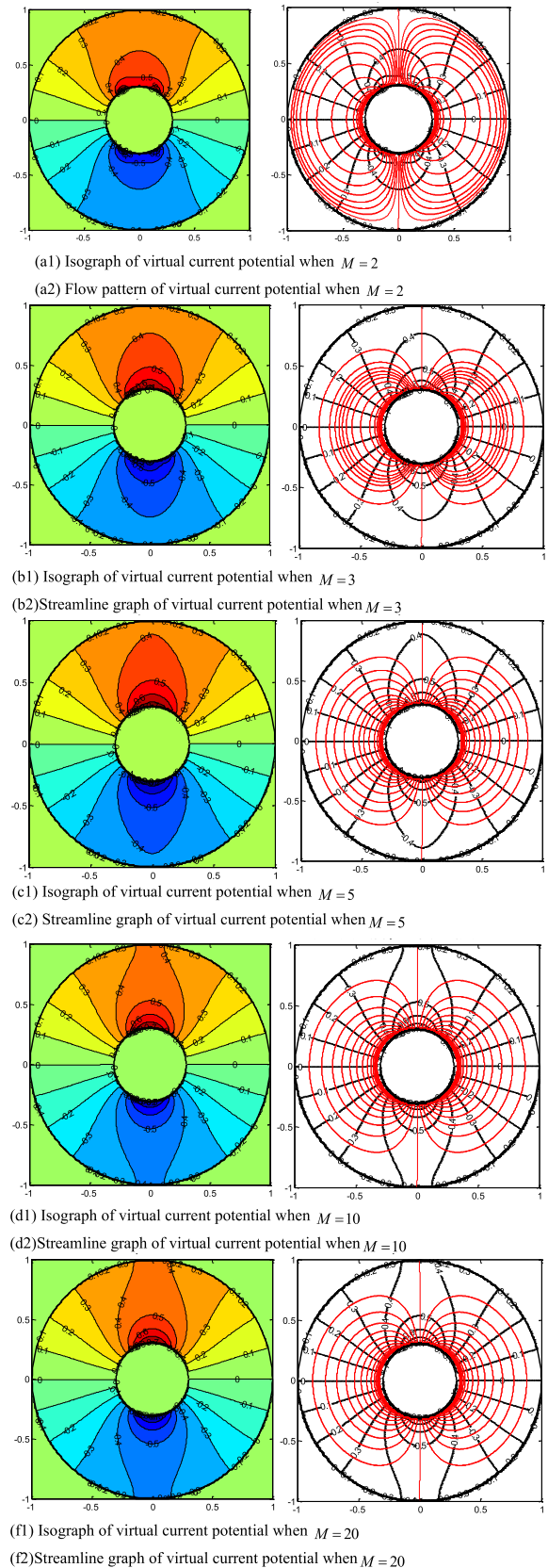

(a1) Isograph of virtual current potential when $M = 2$

(a2) Flow pattern of virtual current potential when $M = 2$

(b1) Isograph of virtual current potential when $M = 3$

(b2) Streamline graph of virtual current potential when $M = 3$

(c1) Isograph of virtual current potential when $M = 5$

(c2) Streamline graph of virtual current potential when $M = 5$

(d1) Isograph of virtual current potential when $M = 10$

(d2) Streamline graph of virtual current potential when $M = 10$

(f1) Isograph of virtual current potential when $M = 20$

(f2) Streamline graph of virtual current potential when $M = 20$

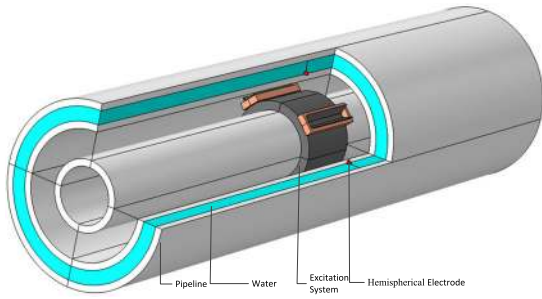**FIGURE 4. Isograph of virtual current potential and flow pattern of virtual current.**

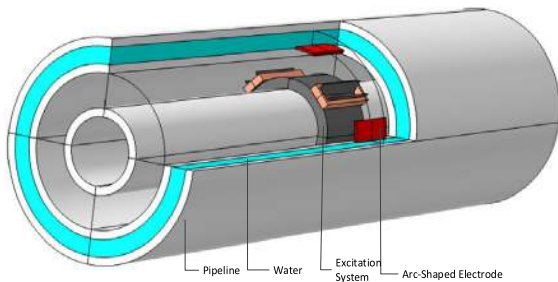**FIGURE 5.** Profile of three-dimensional simulation model (hemisphere electrode).

FIGURE 6. Profile of three-dimensional simulation model (arc electrode).

A. EFFECT OF HEMISPHERE ELECTRODE ON VECTOR WEIGHT FUNCTION

Aiming at the optimal excitation system structure of double coils (5.5 cm in the core protrusion and 2 cm in the core width), when two pairs of hemispherical electrodes are used, and the radius of hemisphere increases from 1 cm to 6.5 cm gradually, the distribution of virtual current and Z-axis weight function can be obtained as shown in Figure 7 and 8. However, according to the simulation model, when the radius of the electrode is greater than 6cm, there will be a cross between the four electrodes, which does not meet the actual electrode installation, so only consider the case of 1cm-6cm.In Figures 7, a, c, e, there are the isograph of virtual current density in XY plane when the radius of hemisphere is 1 cm, 3 cm and 5 cm respectively, and b, d and f are the isogrpahs of virtual current density in YZ plane when the radius of hemisphere is 1 cm, 3 cm and 5 cm respectively. In Figure 8, a, c and e are the X-Y plane equivalence distributions of Z-axis direction weight function when the radius of hemisphere is 1 cm, 3 cm and 5 cm respectively, and b, d and f are the corresponding Y-Z plane equivalence distributions of Z-axis direction weight function.

B. NFLUENCE OF ARC ELECTRODE SHAPE AND SIZE ON THE WEIGHT FUNCTION DISTRIBUTION

Aiming at the optimal excitation system structure of double coils (5.5 cm in the core protrusion and 2 cm in the core width) obtained by the previous simulation, when the arc surface tension angle of the electrode is gradually increased to 80 degrees when the arc surface tension angle of the electrode is 10 degrees, a, C and E in the Figure 9. However,
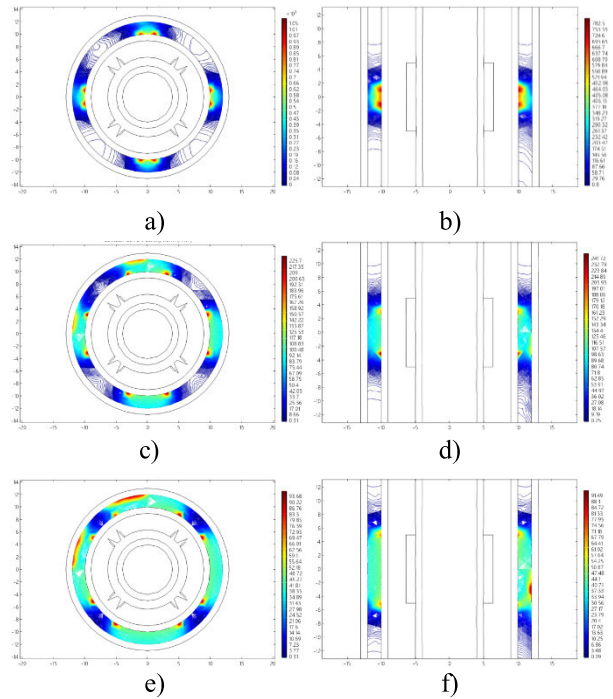

FIGURE 7. Virtual current density isograph when the electrode hemisphere radius are 1cm, 3cm and 5cm.
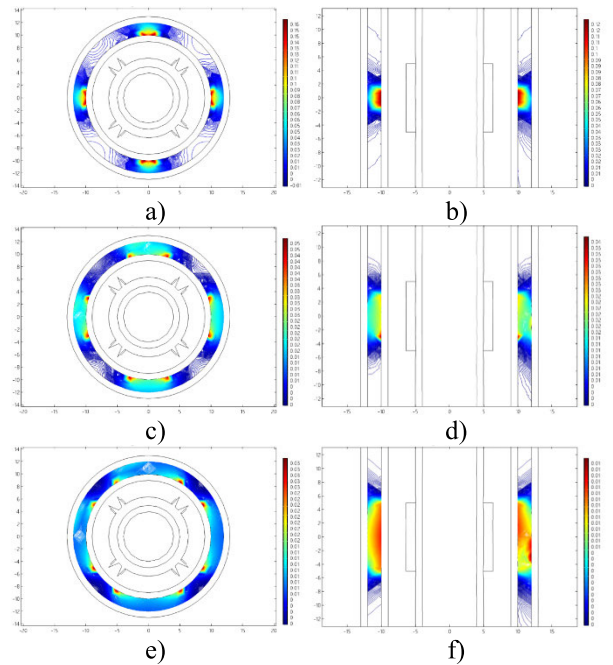

FIGURE 8. weight function isograph in z-axis direction when the electrode hemisphere radius are 1cm, 3cm and 5cm.

according to the simulation model, when the tension angle of the electrode is greater than 70deg, there will be a cross between the four electrodes, which does not meet the actual electrode installation, so only consider the case of 10deg-70deg.There are equivalent distribution maps of virtual current density XY plane (Z = 0) when the arc surface tension
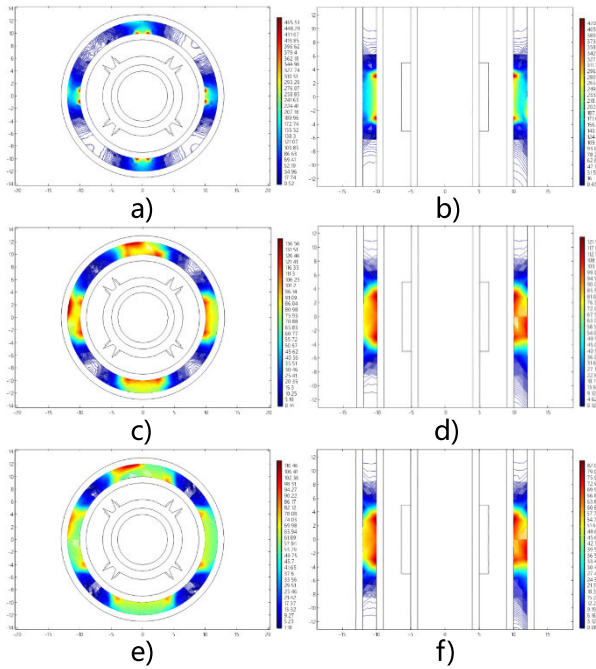
FIGURE 9. Virtual current density equivalent distribution when the electrode arc angle are 10°, 30° and 50°.

FIGURE 10. Weight function isograph in z axis direction wen the electrode arc angles are 30° and 50°.

angle of the electrode is 10 degrees, 30 degrees and 50 degrees respectively, b, d and f are corresponding maps. Equivalent distribution of imaginary current density in YZ plane (X = 0). In Figure 10, a, c and e are equivalent distribution maps of the Z-axis direction weight function XY plane (Z = 0) when the arc tension angles of the electrodes are 10, 30 and 50 degrees respectively, and b, d and f are equivalent distribution maps of the corresponding Z-axis direction weight function YZ plane (X = 0).

IV. RESULT AND ANALYSIS

A. ALUATION SYSTEM

The evaluation for the optimization result is very important. In order to meet the needs of intuitive quantitative analysis, the following three indicators are used for the evaluation of this research work.

1) STANDARD DEVIATION OF VECTOR WEIGHT FUNCTION W_σ

According to the results in the previous section, the purpose of the ideal electrode design is to make W a constant by the excitation system structure design of the electromagnetic flow measurement system. A uniformly distributed W is conducive to the improvement of the measurement accuracy. However, in the practical optimization design, it is very difficult to make W a constant. Therefore, the indexes should be used to evaluate the excitation structure design. In view of the special features of the current electromagnetic flow measurement system of the downhole annular electromagnetic flowmeter and the researches carried out by the scholars around the world [25]–[28], the following indicators can be used to evaluate the weight function σ of the annular flow
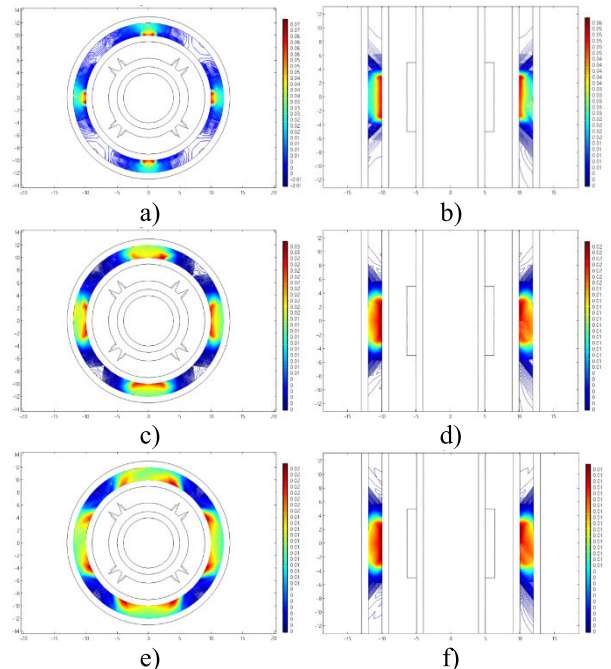
electromagnetic measurement system under different excitation structure, electrode shapes and sizes.

Assuming that a group of vector weight function value is W1, W2, W3$\cdots$ Wi and they are all real numbers, the average of the vector weight function is $\bar{W}$. The standard deviation of the vector weight function W_σ can be expressed by equation (20).

$$W_\sigma = \sqrt{\frac{\sum_{i=1}^{N}(W_i - \overline{W})^2}{N}} \qquad (22)$$

According to the standard deviation equation (20) of the vector weight function, the standard deviation of the vector weight function W_σ is the square sum of the each vector weight function W_i subtracting the average value of the weight function $\bar{W}$. By dividing the result with the N (or N-1, as variance), and taking the square root of the value, the obtained value is the standard deviation W_σ of the vector weight function.

Simply speaking, the standard deviation W_σ of vector weight function is used to describe the average dispersion degree of the vector weight function value. The standard deviation of a larger vector weight function shows that most of the values of vector weight function differ greatly from their average values; a smaller standard deviation of vector weight function values presents that these values are closer to the average of vector weight function values.

2) UNIFORM RANGE RATIO P_e

n order to evaluate the uniformity ratio of vector weight function value distribution in important areas of annular channel, the uniform range ratio is proposed as an evaluation index.

The equation of this index is as follows:

$$\frac{|W_{(x,y)} - \overline{W}|}{\overline{W}} \times 100\% \leq P\% \tag{23}$$

where $W_{(x,y)}$ is the vector weight function value of any finite element in the center crossing section of the annular flow channel; $\overline{W}$s the average of the vector weight function; P is the identified uniform percentage, which can be obtained according to the weight function distributions of the flow channel. In this experiment, P is 30 percent.

If some finite elements satisfy formula (21), it can be considered that the region composed of the points satisfying this condition is the vector weight function w uniform region in the annular channel, while the region composed of the points not satisfying the above formula is the vector weight function w non-uniform region in the annulus channel. Assuming that the number of points constituting the non-uniform region is N1 and the number of points constituting the uniform region is N2, the definition of the proportion of the uniform range can be proposed as shown in equation (22).

$$P_e = \frac{N_2}{N_1 + N_2} \times 100\% \tag{24}$$

More proximity to the constant range ratio indicates a larger uniform area of the annular flow channel weight function W, and is more fitful for the weight function theory of the design requirements. Less proximity to the constant rage illustrates a larger non-uniform region of the vector weight function of the flow channel, and less agreeable for the design requirement of the weight function theory. In practical calculation, considering that the vector weight function mainly concentrates near the electrode, the annular area of the plane where the electrode center is located is taken as the research area.

3) VECTOR WEIGHT FUNCTION OF COEFFICIENT VARIATION CV

Coefficient of variation, also known as standard deviation rate, is another statistic used to measure the degree of variation of each observed value in a sample. When comparing the degree of variation of two or more samples, if the unit of measurement is the same as the average, the standard deviation can be directly used for comparison [29]. If the unit and/or average are different, the standard deviation can not be used to compare the degree of variation, but the ratio of standard deviation to average should be used for comparison. In this study, the coefficient of variation is compared with the vector weight function, and its coefficient of variation can be defined as follows:

$$C_v = \frac{W_\sigma}{\overline{W}} \tag{25}$$

It can be considered that the coefficient of variation of the vector weight function, like the standard deviation, reflects the discreteness of the vector weight function data. The data size is affected not only by the discrete degree of variable values, but also by the average level of variable values. Therefore, the smaller the coefficient of variation of the vector
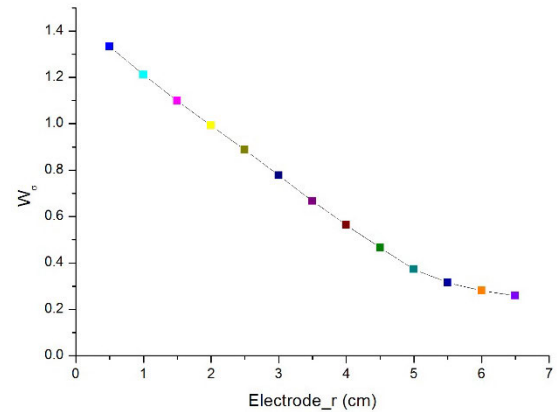

FIGURE 11. Standard deviation trend diagram of vector weight function when the radius of electrode hemisphere varies.

weight function is, the greater the discreteness of the vector weight function is, and the better the optimization effect is.

B. SIMULATION DATA ANALYSIS

1) HEMISPHERE ELECTRODE SIMULATION DATA ANALYSIS

Figure 7 and 8 show that when the radius of the electrode hemisphere changes, the distribution of virtual current density and vector weight function in annular fluid domain will change significantly. It is found that the distribution range of virtual current density is 0.09-91.49A/m2 when the radius of electrode is 5 cm, and the distribution range of vector weight function is the smallest, ranging from 0 to 0.03. When the radius of electrode is 1 cm, the distribution range of virtual current density is 0.8-782.5A/m2, and the distribution range of vector weight function is the largest, ranging from - 0.01 to 0.16. Increasing the radius will reduce the distribution norm of vector weight function range.

In order to quantitatively analyze the influence of electrode hemisphere radius on annular flow electromagnetic measurement system, 12 cases with electrode hemisphere radius ranging from 0.5 cm to 6 cm were scanned and analyzed. The standard deviation of vector weight function was solved by using the derivative function of COMSOL. Figure 11 was obtained. As shown in Figure 11, the standard deviation of the vector weight function decreases from 1.33 to 0.26 with the increase of the hemispheric radius of the electrode, which improves the measurement accuracy of the system.

Similarly, based on the simulation data and corresponding calculation, the uniform range ratio and weight function variation can be obtained. The variation graphs are shown in Figure 12 and 13.

According to Figure 12 and 13, it can be seen that increasing the radius of hemispherical electrode can improve the proportion of uniform range and decrease the coefficient of variation of vector weight function. When the radius of the hemispherical electrode is 6 cm, the standard deviation of the vector weight function is the smallest, the proportion of uniform range is the largest, and the coefficient of variation of the vector weight function is the smallest. Therefore,
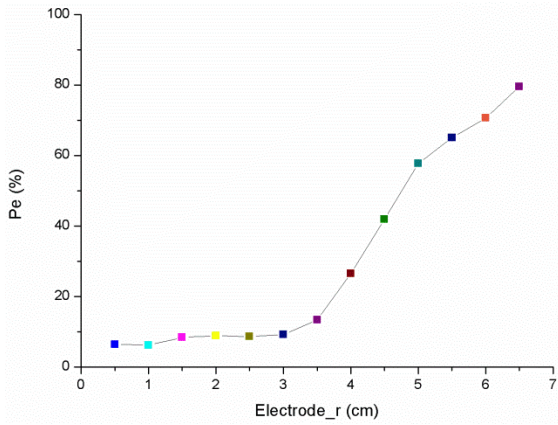
FIGURE 12. Uniform range ratio analysis when the electrode hemisphere varies.
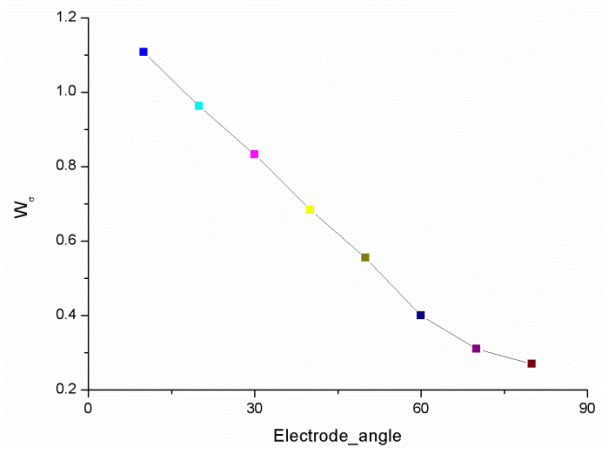

FIGURE 13. Analysis curve of variation coefficient of vector weight Function when the hemisphere radius varies.

FIGURE 14. Trend chart of standard deviation table of vector weight function when arc tension angle of electrode changes.
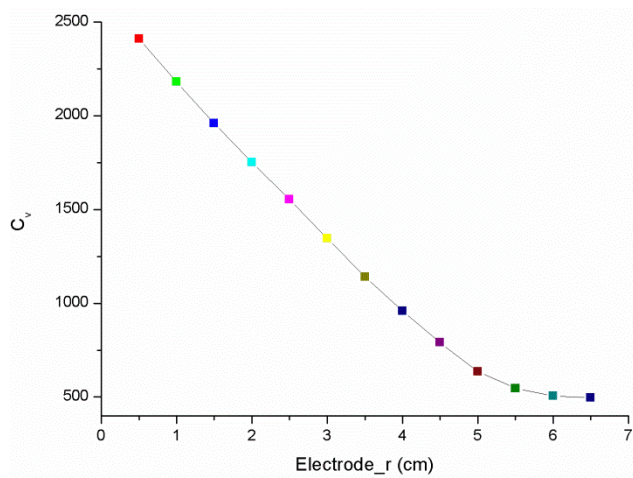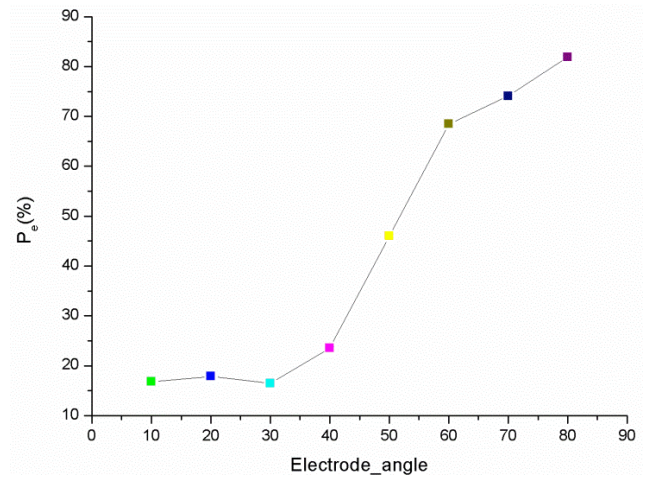

FIGURE 15. Proportional analysis of uniform range of arc angle of electrode.

FIGURE 16. Analysis of variation coefficient of vector weight function with variation of arc angle of electrode.

considering the three indexes synthetically, for the hemispherical electrode, 6 cm is the optimal electrode design in the current structure space.

2) ARC ELECTRODE SIMULATION DATA ANALYSIS

It is shown from Figure 9 and 10 that when the arc angle of the electrode changes, the distribution of virtual current density and vector weight function in annular fluid domain will change significantly. It is found that the distribution range of virtual current density is 0.08-82.05A/m2 when the arc angle of the electrode is 50 degrees, and the distribution range of vector weight function is the smallest, ranging from 0 to 0.02. When the arc angle of the electrode is 10 degrees, the distribution range of virtual current density is 0.43-420.68A/m2, and the distribution range of vector weight function is the largest, ranging from -0.01 to 0.07. Increasing the radius will reduce the vector distribution range of weight function.

In order to quantitatively analyze the influence of the arc angle of the electrode on the annular flow electromagnetic measurement system, seven cases of the arc angle of the elec-
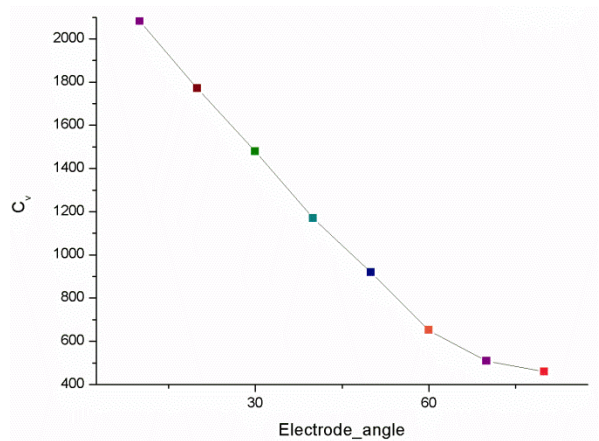
trode are scanned and analyzed under the condition of 10 deg to 70 deg respectively. The standard deviation of the vector weight function is solved by using the derivative function of

COMSOL. Figure 14 is obtained. From Figure 14, it can be seen that the standard deviation of the vector weight function decreases from 1.11 to 0.27 with the increasing of the arc angle of the electrode, which improves the measurement accuracy of the system.

Similarly, based on the simulation data and corresponding operations, the variation curves of the uniform range ratio and the coefficient of variation of the vector weight function can be obtained as shown in Figure 15 and Figure 16, respectively.

As shown in Figure 15 and Figure 16, increasing the tension angle of arc surface electrode can improve the proportion of uniform range and decrease the coefficient of variation of vector weight function. When the tension angle of the arc surface electrode is 70 deg, the standard deviation of the vector weight function is the smallest, the proportion of the uniform range is the largest, and the coefficient of variation of the vector weight function is the smallest. The three evaluation indexes all reach the optimal value. Therefore, considering the three indexes synthetically, for the arc surface electrode, the tension angle of 70 deg is the optimal electrode design in the current structure space.

V. CONCLUSION

In this study, the electrodes of electromagnetic measurement system for downhole annular flow in drilling engineering are optimized, which lays a foundation for the realization of electromagnetic measurement instrument for downhole annular flow in the future. The main research work of this paper is as follows:

(1) Based on Bevir's vector weight function theory, the partial differential equation of annular flow electromagnetic measurement system is established. According to different boundary conditions, the virtual current potential and virtual current density of annular channel electromagnetic flow measurement system are solved, and the distribution law of virtual current density of hemispherical and arc electrodes is obtained.

(2) Based on the theoretical study of hemispherical and arc electrodes, the weight functions of hemispherical and arc electrodes are simulated by finite element method. For the hemispherical electrode, 6 cm is the optimal electrode design in the current structure space. For the arc surface electrode, the tension angle of 70 deg is the optimal electrode design in the current structure space.

(3) Three evaluation indexes are proposed to analyze and evaluate the simulation data, and the optimal design parameters of hemispherical and arc electrodes in the current structure space are obtained.

REFERENCES

[1] H. Santos, C. Leuchtenberg, and S. Shayegi, "Micro-flux control: The next generation in drilling process," in *Proc. SPE Latin Amer. Caribbean Petroleum Eng. Conf. Soc. Petroleum Eng.*, 2003, pp. 12–19.

[2] K. Ling, J. He, J. Ge, P. Pei, and Z. Shen, "A rigorous method to calculate the rising speed of gas kick," *J. Petroleum Explor. Prod. Technol.*, vol. 5, no. 1, pp. 81–89, Mar. 2015.

[3] L. Ge, G. Wei, Q. Wang, Z. Hu, and J. Li, "Novel annular flow electromagnetic measurement system for drilling engineering," *IEEE Sensors J.*, vol. 17, no. 18, pp. 5831–5839, Sep. 2017.

[4] J. Guan, H. Zhang, and C. Hu, "Multi-electrode electromagnetic flowmeter," in *Proc. Int. Symp. Instrum. Sci. Technol.*, 2002, pp. 69–75.

[5] N. Rajabi, "Droplet actuation on various electrode shapes in electrowetting-based microfluidics," *Colloids Surf. A, Physicochem. Eng. Aspects*, vol. 365, no. 10, pp. 230–236, 2009.

[6] N. Rajabi and A. Dolatabadi, "A novel electrode shape for electrowetting-based microfluidics," *Colloids Surf. A, Physicochem. Eng. Aspects*, vol. 365, nos. 1–3, pp. 230–236, Aug. 2010.

[7] S. Yin, B. Li, K. Meng, and J. Chen, "Performance differences of an electromagnetic flow sensor with nonideal electrodes based on different-dimensional weight functions," *IEEE Trans. Instrum. Meas.*, vol. 67, no. 7, pp. 1738–1748, Jul. 2018.

[8] B. Horner, "A novel profile-insensitive multi-electrode induction flowmeter suitable for industrial use," *Measurement*, vol. 24, no. 3, pp. 131–137, Oct. 1998.

[9] G. P. Lucas, J. C. Cory, and R. C. Waterfall, "A six-electrode local probe for measuring solids velocity and volume fraction profiles in solids-water flows," *Meas. Sci. Technol.*, vol. 11, no. 10, pp. 1498–1509, 2000.

[10] X.-Z. Zhang and Y. Li, "Calculation of the virtual current in an electromagnetic flow meter with one bubble using 3D model," *ISA Trans.*, vol. 43, no. 2, pp. 189–194, Apr. 2004.

[11] H. J. Zhang, J. Guan, and H. U. Chi-Ying, "Flow measurement with multielectrode based on electromagnetic induction principle," *Acta Metrologica Sinica*, vol. 25, no. 1, pp. 43–46, 2004.

[12] G. Y. Zhang, B. L. Liu, and L. I. Long-Qiu, "Simulation and experimental study on four-electrode outflow electromagnetic flowmeter," *J. Hebei Univ. Sci. Technol.*, vol. 32, no. 5, pp. 441–445, 2011.

[13] Y. Y. Zhao, T. Zhang, and G. Lucas, "Electrode design of multi-electrode electromagnetic flow meter based on region weight function theory," *Transducer Microsyst. Technol.*, vol. 33, no. 2, pp. 94–97, 2014.

[14] J. A. Shercliff, *Electromagnetic Flow-Measurement*. Cambridge, U.K.: Cambridge Univ. Press, 1962.

[15] T. Leeungculsatien and G. P. Lucas, "Measurement of velocity profiles in multiphase flow using a multi-electrode electromagnetic flow meter," *Flow Meas. Instrum.*, vol. 31, no. 6, pp. 86–95, Jun. 2013.

[16] L. E. Kollár, G. P. Lucas, and Z. Zhang, "Proposed method for reconstructing velocity profiles using a multi-electrode electromagnetic flow meter," *Meas. Sci. Technol.*, vol. 25, no. 7, Jul. 2014, Art. no. 075301.

[17] Y. Shi, M. Wang, M. Shen, and H. Wang, "Optimization of an electromagnetic flowmeter for dual-parameter measurement of vertical air-water flows," *J. Mech. Sci. Technol.*, vol. 29, no. 7, pp. 2889–2895, Jul. 2015.

[18] L. F. Kong, S. X. Du, and Y. W. Li, "Simulation research on weight function of multi-electrode electromagnetic flowmeter," *Acta Metrologica Sinica*, vol. 36, no. 1, pp. 58–62, 2015.

[19] L. Ge, H. Li, Q. Huang, G. Tian, G. Wei, Z. Hu, and J. Ahmed, "Electromagnetic flow detection technology based on correlation theory," *IEEE Access*, vol. 8, pp. 56203–56213, 2020.

[20] L. Ge, Y. He, G. Tian, G. Wei, J. Ahmed, H. Deng, and Q. Huang, "Measurement of annular flow for drilling engineering by electromagnetic flowmeter based on double-frequency excitation," *J. Sensors*, vol. 2019, pp. 1–14, Nov. 2019.

[21] L. Ge, H. Deng, Q. Wang, Z. Hu, and J. Li, "Study of the influence of temperature on the measurement accuracy of transit-time ultrasonic flowmeters," *Sensor Rev.*, vol. 39, no. 2, pp. 269–276, Mar. 2019.

[22] M. K. Bevir, "The theory of induced voltage electromagnetic flowmeters," *J. Fluid Mech. Digit. Arch.*, vol. 43, no. 3, p. 14, 1970.

[23] L. Ge, H. Li, Q. Wang, G. Wei, Z. Hu, J. Liao, and J. Li, "Design and optimization of annular flow electromagnetic measurement system for drilling engineering," *J. Sensors*, vol. 17, no. 18, pp. 5831–5839, 2018.

[24] L. Ge, D. Li, J. Liao, Z. Hu, and G. Wei, "Optimization of downhole annular electromagnetic flowmeter measurement system with single electrode," *Eng. Sci. Technol.*, vol. 50, no. 4, pp. 237–245, 2018.

[25] N. D. Jin, Y. B. Zong, Y. H. Zhang, and J. Li, "Numerical simulation of magnetic field distribution characteristics of the four-electrode electromagnetic flowmeter," *Ind. Meas.*, vol. 19, no. 2, pp. 2–6, 2009.

[26] A. Michalski, J. Starzynski, and S. Wincenciak, "3-D approach to designing the excitation coil of an electromagnetic flowmeter," *IEEE Trans. Instrum. Meas.*, vol. 51, no. 4, pp. 833–839, Aug. 2002.

[27] V. Sharma, G. V. Kumar, S. K. Dash, B. K. Nashine, and K. K. Rajan, "Modeling of permanent magnet flowmeter for voltage signal estimation and its experimental verification," *Flow Meas. Instrum.*, vol. 28, pp. 22–27, Dec. 2012.

[28] J.-F. Liu, H. Choi, and M. Walmer, "Design of permanent magnet systems using finite element analysis," *J. Iron Steel Res., Int.*, vol. 13, pp. 383–387, Jan. 2006.

[29] M. Shi, L. Feng, Z. Huang, M. Zhang, H. Wen, and Q. Liu, "Defect detection of oil and gas pipeline using remote field eddy current technology," *J. Magn.*, vol. 24, no. 3, pp. 530–542, Sep. 2019.

LIANG GE received the Ph.D. degree, in 2017. He is currently an Associate Professor with the College of Mechanical and Electronic Engineering, Southwest Petroleum University. His current research interests include downhole instruments and petroleum devices.

DAN LI received the B.S. degree from Southwest Petroleum University, Chengdu, China, in 2016, where he is currently pursuing the M.E. degree in measuring, and testing technology and instrument.

QI HUANG (Student Member, IEEE) is currently pursuing the bachelor's degree with the Electrical and Mechanical Department, Southwest Petroleum University, Chengdu, China. His current research interests include electromagnetic flow measurement and nondestructive testing.

GUIYUN TIAN (Senior Member, IEEE) received the Ph.D. degree from the University of Derby, Derby, U.K., in 1998. Since 2007, he has been the Chair Professor of sensor technologies with Newcastle University, Newcastle upon Tyne, U.K. He has coordinated several research projects from the Engineering and Physical Sciences Research Council, the Royal Academy of Engineering, and FP7, and has good collaboration with leading industrial companies, such as Airbus, Rolls Royce, BP, nPower, and TWI.

GUOHUI WEI received the B.S. degree in physics from Northwest Normal University and the M.E. degree in radio physics from Xidian University, in 1998 and 2006, respectively.

JUNAID AHMED received the M.S. degree in electrical and electronics engineering from Eastern Mediterranean University (EMU), North Cyprus, Turkey, in 2015. He is on study leave for the Ph.D. degree in non-destructive testing and structural health monitoring from the School of Automation Engineering, UESTC, Chengdu, China. His current research interests include quantitative non-destructive testing and evaluation, sparse representations, and low rank matrix and tensor factorizations.

● ● ●